Ezrin tunes T-cell activation by controlling Dlg1 and microtubule positioning at the immunological synapse

Rémi Lasserre[1,2,14], **Stéphanie Charrin**[1,2,14,15], **Céline Cuche**[1,2], **Anne Danckaert**[3], **Maria-Isabel Thoulouze**[1,2], **Fabrice de Chaumont**[4,5], **Tarn Duong**[6,16], **Nathalie Perrault**[7,8,9,10], **Nadine Varin-Blank**[7,8,9,10,17], **Jean-Christophe Olivo-Marin**[4,5], **Sandrine Etienne-Manneville**[5,11], **Monique Arpin**[12,13], **Vincenzo Di Bartolo**[1,2] and **Andrés Alcover**[1,2,*]

[1]Institut Pasteur, Department of Immunology, Lymphocyte Cell Biology Unit, Paris, France, [2]CNRS, URA1961, Paris, France, [3]Institut Pasteur, Dynamic Imaging Platform, Imagopole, Paris, France, [4]Institut Pasteur, Department of Cell Biology and Infection, Quantitative Image Analysis Unit, Paris, France, [5]CNRS, URA-2582, Paris, France, [6] Institut Pasteur, Department of Cell Biology and Infection, Imaging and Modeling Group, Paris, France, [7]Institut Cochin, Department of Hematology, Paris, France, [8]CNRS UMR8104, Paris, France, [9]Université Paris Decartes, Paris, France, [10]INSERM, U567, Paris, France, [11]Institut Pasteur, Department of Cell Biology and Infection, Cell Polarity and Migration Group, Paris, France, [12]Institut Curie, Morphogenesis and Cell Signalling Laboratory, Paris, France and [13]CNRS, UMR144, Paris, France

T-cell receptor (TCR) signalling is triggered and tuned at immunological synapses by the generation of signalling complexes that associate into dynamic microclusters. Microcluster movement is necessary to tune TCR signalling, but the molecular mechanism involved remains poorly known. We show here that the membrane-microfilament linker ezrin has an important function in microcluster dynamics and in TCR signalling through its ability to set the microtubule network organization at the immunological synapse. Importantly, ezrin and microtubules are important to down-regulate signalling events leading to Erk1/2 activation. In addition, ezrin is required for appropriate NF-AT activation through p38 MAP kinase. Our data strongly support the notion that ezrin regulates immune synapse architecture and T-cell activation through its interaction with the scaffold protein Dlg1. These results uncover a crucial function for ezrin, Dlg1 and microtubules in the organization of the immune synapse and TCR signal down-regulation. Moreover, they underscore the importance of ezrin and Dlg1 in the regulation of NF-AT activation through p38.

Introduction

Immunological synapses are organized cell contacts between T lymphocytes and antigen-presenting cells (APC). They form upon T-cell receptor (TCR) engagement with peptide antigens bound to major histocompatibility complex molecules displayed on the APC surface (Dustin, 2008). TCR triggering is rapidly followed by the generation of signalling complexes that nucleate at the immunological synapse forming dynamic microclusters composed of TCR subunits and various signalling effectors, including the adaptors SLP-76 and LAT, and the ZAP-70 protein tyrosine kinase. Microclusters nucleate at the periphery of the immunological synapse, in which signalling is initiated and then move towards the centre of the synapse in which the activation signal is extinguished (Bunnell *et al*, 2002; Mossman *et al*, 2005; Yokosuka *et al*, 2005; Barr *et al*, 2006; Varma *et al*, 2006; Nguyen *et al*, 2008). Therefore, the topology and dynamics of signalling complexes seem critical to trigger and tune TCR signalling.

Interactions between plasma membrane components, signalling molecules and the actin cytoskeleton are important to coordinate in time and space the signal transduction machinery that connects the TCR with downstream activation events (Burkhardt *et al*, 2008). Various findings support the involvement of membrane-microfilament linkers of the ezrin, radixin, moesin (ERM) family in molecular reorganization at the immunological synapse (Charrin and Alcover, 2006; Burkhardt *et al*, 2008). A function of ERMs in cortical cytoskeleton relaxation (Faure *et al*, 2004), CD43 exclusion from the immunological synapse (Allenspach *et al*, 2001; Delon *et al*, 2001; Savage *et al*, 2002; Ilani *et al*, 2007), TCR clustering (Roumier *et al*, 2001) and B-cell receptor diffusion dynamics at the plasma membrane (Treanor *et al*, 2010) has been proposed. Over-expression of the ezrin FERM domain, or genetic inactivation of ezrin, impairs NF-AT activation and IL2 production (Allenspach *et al*, 2001; Roumier *et al*, 2001; Shaffer *et al*, 2009). The respective functions of ezrin and moesin in immunological synapse formation and in T-cell activation remain, however, unclear (Ilani *et al*, 2007; Shaffer *et al*, 2009).

ERMs are ubiquitous multifunctional proteins involved in cellular architecture, cell motility, protein localization and intracellular signalling. ERMs display a homologous

*Corresponding author. Unité de Biologie Cellulaire des Lymphocytes, Institut Pasteur, 28, rue Docteur Roux, 75724 Paris Cedex 15, France. Tel: +33 1 40 61 30 64; Fax: +33 1 45 68 89 29; E-mail: andres.alcover@pasteur.fr
[14]These authors contributed equally to this work
[15]Present address: INSERM U602, Institut André Lwoff, Hôpital Paul Brousse, Villejuif F-94807, France
[16]Present address: UMR144 CNRS, Institut Curie, Paris F-75005, France
[17]Present address: UMR U978 INSERM/Université Paris 13, UFR SMBH, Bobigny F-93017, France

N-terminal FERM domain, which interacts with membrane phospholipids, trans-membrane proteins (i.e. ICAMs, CD43, CD44) and signalling molecules. Moreover, ERMs interact with F-actin through their C-terminal region (Charrin and Alcover, 2006; Fievet *et al*, 2007; Fehon *et al*, 2010). ERMs exist in equilibrium between a 'closed' conformation in which the FERM and the C-terminal domains interact quenching protein interaction sites, and an 'open' conformation favouring interactions through the FERM domain and with the actin cytoskeleton. The open conformation is favoured by phosphoinositide binding and by the phosphorylation of a threonine residue in the C-terminal region (Fievet *et al*, 2004). TCR activation induces the rapid dephosphorylation and rephosphorylation of this threonine in both ezrin and moesin (Delon *et al*, 2001; Faure *et al*, 2004; Ilani *et al*, 2007). Ezrin can interact mainly through its FERM domain with a variety of signalling molecules (Takahashi *et al*, 1997; Ng *et al*, 2001; Poullet *et al*, 2001; Perez *et al*, 2002; Urzainki *et al*, 2002; Pujuguet *et al*, 2003; D'Angelo *et al*, 2007; Ilani *et al*, 2007; Ruppelt *et al*, 2007; Naba *et al*, 2008).

The mammalian homologue of the Drosophila Disc large protein (Dlg1, Dlgh1, hDlg) is an ubiquitous PDZ-domain-containing scaffold protein of the MAGUK family. It is relocalized to the immunological synapse, it associates with various TCR signalling molecules, such as Lck, ZAP-70, TCRζ and WASP and is implicated in NF-AT activation and cytokine production (Xavier *et al*, 2004; Ludford-Menting *et al*, 2005; Round *et al*, 2005). The effect of Dlg1 on NF-AT activation is due to its ability to interact with and regulate the activity of the p38 MAP kinase (Round *et al*, 2007). Moreover, Dlg1 associates through its PDZ-1 and PDZ-2 domains, or its I3 domain with erythrocyte band 4.1 and ezrin FERM domains, but not with moesin or radixin (Lue *et al*, 1996). Finally, Dlg1 is also known as part of a complex of cell polarity regulators that control microtubule positioning in migrating cells (Etienne-Manneville *et al*, 2005).

We investigated here the function of ezrin in molecular dynamics at the immunological synapse and in TCR signalling. Ezrin silencing perturbs the localization and movement of signalling microclusters by perturbing the microtubule network organization at the immunological synapse. Importantly, ezrin silencing impairs the control of TCR-proximal signalling events leading to enhanced Erk1/2 activation. In addition, ezrin is required for appropriate NF-AT activation. We propose that ezrin performs this dual regulation of T-cell activation through its interaction with the scaffold protein Dlg1. Our data unveil an important function of ezrin and Dlg1 in structuring the immunological synapse and in the regulation of T-cell activation.

Results

Ezrin silencing impairs signalling microcluster dynamics
TCR triggering is followed by the generation of microclusters containing TCR as well as signalling effectors, such as SLP-76, LAT and ZAP-70. The generation and dynamics of signalling microclusters depend on functional interactions between the TCR, the signal transduction machinery and the actin cytoskeleton (Dustin, 2008). As ezrin links plasma membrane components with filamentous actin and is redistributed to the immunological synapse (Roumier *et al*, 2001; Ilani *et al*,

2007), we hypothesized that ezrin could modulate signalling microcluster dynamics. We, therefore, specifically silenced ezrin expression using siRNA (Figure 1A) and we studied the dynamics of SLP-76-containing signalling microclusters. SLP-76 is a central scaffold molecule of the TCR signalling cascade (Acuto *et al*, 2008), which is rapidly recruited from the cytosol to microclusters that then move from the periphery to the centre of the immunological synapse (Bunnell *et al*, 2002; Campi *et al*, 2005; Yokosuka *et al*, 2005).

SLP-76-deficient Jurkat J14 cells stably expressing YFP-SLP-76 were transfected with control (siCont) or siEzrin (siEz) oligonucleotides. Three days later, cells were plated on anti-CD3-coated coverslips and SLP-76 was tracked by live cell imaging. As earlier described by others (Yokosuka *et al*, 2005; Varma *et al*, 2006), SLP-76 microclusters were generated in two phases. A first one, concomitant with cell expansion, occurred soon after cell contact with the stimulatory surface, and was characterized by the formation of microcluster aggregates at the initial contact sites. A second phase occurred on cell spreading and was characterized by microcluster nucleation at the periphery of the synapse followed by continuous movements of microclusters towards the centre (Supplementary Movie 1). SLP-76 microclusters dissipated before reaching the centre of the synapse (Supplementary Movie 1) (Bunnell *et al*, 2002; Yokosuka *et al*, 2005). In ezrin-silenced cells, the first phase of SLP-76 microclusters seemed to occur normally, whereas the second phase seem not to take place. Thus, SLP-76 microclusters rapidly formed, but remained aggregated and did not undergo centripetal movements (Supplementary Movie 2). The differences were readily seen in '3D + time' projections and in kymographs. Control cells displayed radial trajectories and convergent kymograph lines (Figure 1B, top and bottom, respectively), whereas ezrin-silenced cells showed disconnected microcluster areas and parallel kymograph lines (Figure 1C, top and bottom, respectively). Similar results were obtained with another siRNA oligonucleotide, ruling out possible off target effects (Figure 1D). On the basis of movies and 3D + time projections, we classified the cells in three categories: phenotype 1 represented cells displaying microclusters with radial trajectories, phenotype 3 represented cells with microclusters undergoing short or undetectable trajectories and remaining in separate zones and phenotype 2 was intermediate between 1 and 3. Control cells mostly fitted with phenotype 1, and ezrin-silenced cells with phenotype 3 (Figure 1E).

To further investigate the relationship between ezrin silencing and altered SLP-76 microcluster dynamics, we fixed the cells at two different times and we analysed the location of SLP-76 microclusters, as well as the presence of phosphorylated LAT at Tyr[191] (pLAT). Consistent with live cell data (Supplementary Movie 1), at 1 min of contact, SLP-76 microclusters appeared grouped in several contact zones in both control and ezrin-silenced cells. SLP-76 microcluster aggregates were also enriched in pLAT (Figure 2A and B). At 3 min, most control cells generated numerous microclusters that appeared as SLP-76 and pLAT positive puncta evenly distributed over the contact surface (Figure 2C). In contrast, ezrin-silenced cells displayed SLP-76 microclusters forming several aggregates in which pLAT was enriched (Figure 2D). Quantitative image analysis confirmed that SLP-76 microclusters were more aggregated in ezrin-silenced cells than in control cells (Figure 2E). Similarly, ezrin-silenced primary CD4 T cells
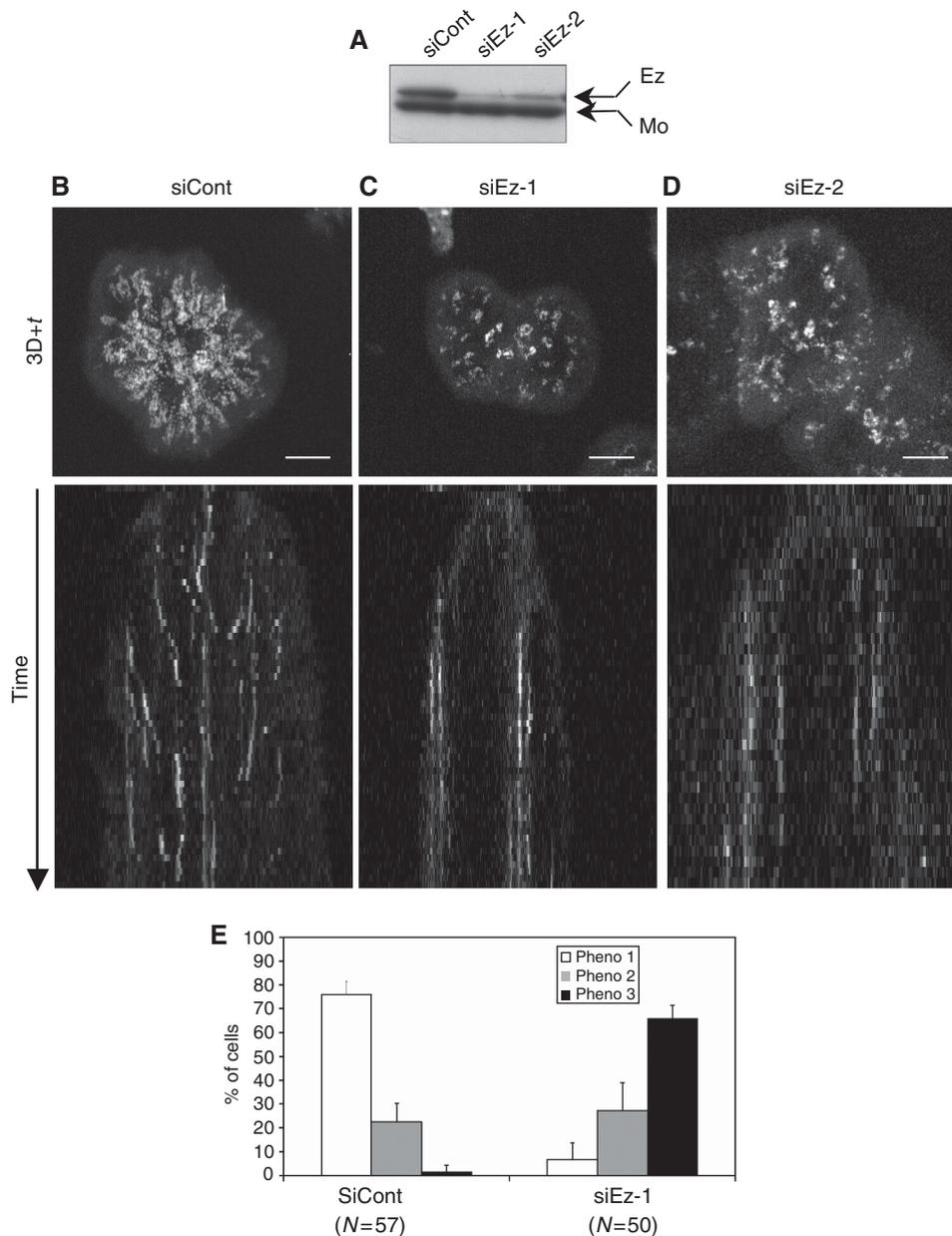
Figure 1 Ezrin silencing alters SLP-76 microcluster dynamics. Jurkat J14 cells expressing YFP-SLP-76 and transfected with siRNA control or with two different siRNA ezrin oligonucleotides (siEz-1 and siEz-2) were activated on anti-CD3-coated coverslips and subjected to live cell imaging using a spinning disc confocal microscope. (**A**) Total cell lysates were analysed by western blot with pooled anti-ezrin and anti-moesin Abs. Inhibition of ezrin expression was ~80% for oligo 1 and ~70% for oligo 2. (**B–D**, top panels) Projection of 3D + time images of YFP-SLP-76 microclusters recorded during 5 min at 12 images/min. (**B–D**, bottom panels) Kymograph representation of YFP-SLP-76 events occurring within an 8 pixel band located in the middle of each cell. Note that kymograph patterns in control cells converged towards the centre, whereas in ezrin-silenced cells remained parallel. (**E**) Using movies and 3D + time projections, cells were classified in three categories. Phenotype 1 corresponds to cells in which SLP-76 microclusters displayed centripetal movements (**B**; Supplementary Movie 1). Phenotype 3 corresponds to cells in which SLP-76 microclusters stayed rather immobile within the same subcellular areas (**C**; Supplementary Movie 2). Phenotype 2 corresponds to intermediate states between phenotype 1 and 3. A representative experiment is shown out of five independent experiments for (**B**), (**C**) and (**E**) and two for (**D**). Histograms in (**E**) show data from five independent experiments ± s.d. Scale bar = 5 μm.

from healthy donors exhibited more frequently pLAT microcluster aggregates, as well as more irregular shapes than control cells (Figure 2G–I).

Consistent results were obtained when general phosphotyrosine (pTyr) detection was performed (Supplementary Figure 1A and B). In ezrin-silenced cells, pTyr appeared present not only in SLP-76-containing puncta, but also in less defined large structures to which the SLP-76 puncta seemed connected (Supplementary Figure 1B, right panels).

Finally, ezrin silencing also altered the pattern of microclusters containing TCRζ (Supplementary Figure 1C), indicating that the effect of ezrin silencing was not exclusive of SLP-76 and LAT.

We next assessed whether ezrin was part of signalling microclusters. As shown in Supplementary Figure 1D, ezrin was not enriched in SLP-76 microclusters, suggesting that the effect of ezrin silencing on microcluster dynamics was unlikely due to the involvement of ezrin in these structures.
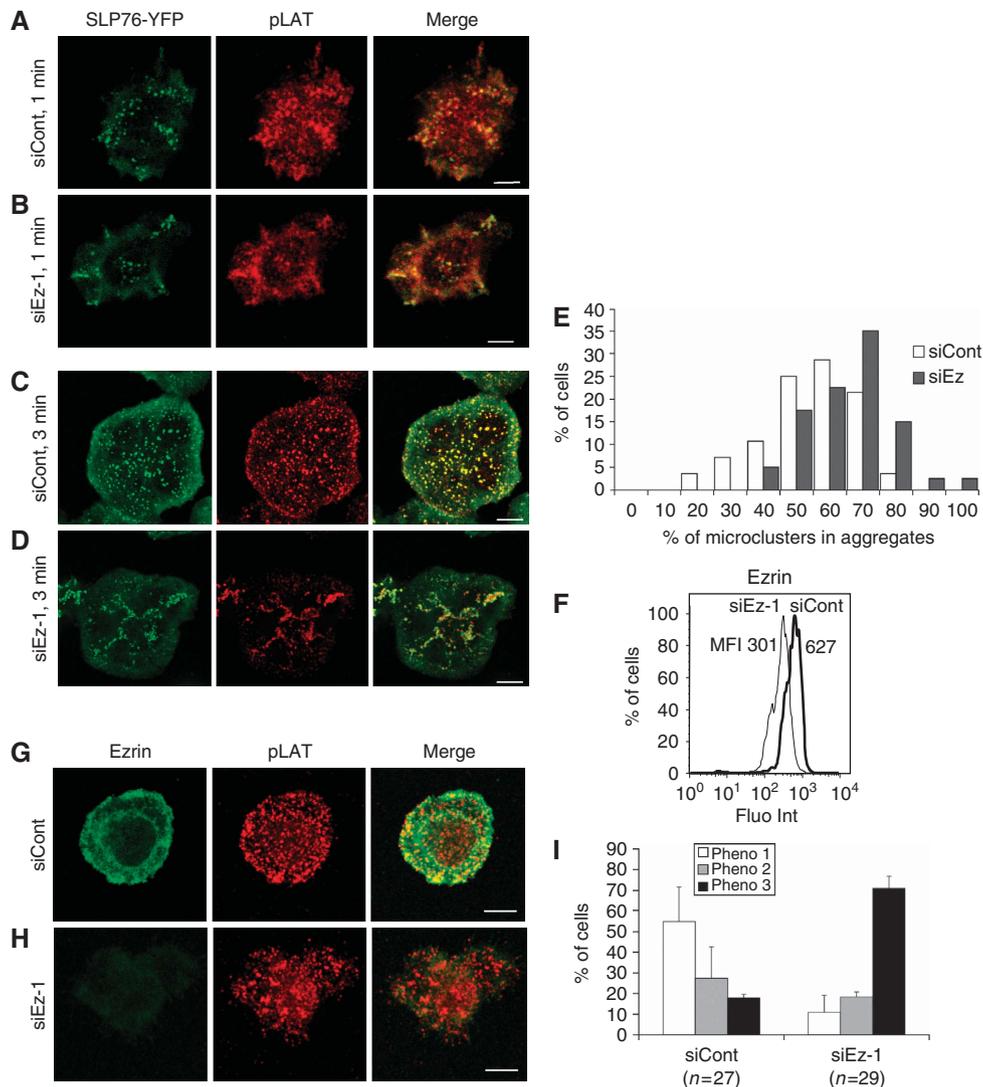
Figure 2 Ezrin silencing alters the pattern of signalling microclusters. (**A–D**) Jurkat J14 cells expressing YFP-SLP-76 and transfected with siRNA control or siRNA ezrin-1 were activated on anti-CD3-coated coverslips for 1 or 3 min, fixed, stained with anti-phospho-LAT (pTyr[191]) Abs and analysed by confocal microscopy. An optical section at the contact surface is shown. One representative experiment out of five is shown. (**E**) The percentage of SLP-76 microclusters within aggregates was measured by quantitative image analysis, as described in Materials and methods, and plotted versus the percentage of cells displaying various degrees of aggregation. Ezrin-silenced cells displayed significant higher percentage of microcluster aggregates ($P = 0.003$). (**F–I**) Human primary CD4 T cells were transfected with siRNA control, or siRNA ezrin-1 and processed as follows: (**F**) Primary T cells were fixed, permeabilized, stained with anti-ezrin Abs and analysed by flow cytometry. Mean fluorescence intensity (MFI) is indicated. Ezrin expression in ezrin-silenced cells was reduced by 50%. (**G, H**) Primary T cells were activated on anti-CD3 + anti-CD28-coated coverslips for 5 min, fixed, permeabilized, stained with anti-ezrin and anti-phospho-LAT (pTyr[191]) Abs, and analysed by confocal microscopy. An optical section at the contact surface is shown. (**I**) Primary T cells were classified in three categories. Phenotype 1 corresponds to cells displaying a regular shape and a homogeneous pattern of pLAT microclusters (**G**). Phenotype 3 corresponds to cells displaying irregular shapes and an aggregated pattern of pLAT microclusters (**H**). Phenotype 2 corresponds to intermediate patterns. One representative experiment is shown out of three. Plots show data from three independent experiments ± s.d. Scale bar = 5 µm.

In agreement with the data obtained on activatory planar surfaces, pSLP-76/pLAT microcluster patterns in T-cell-APC immunological synapses were also altered by ezrin silencing. Thus, microclusters were more aggregated in ezrin-silenced cell synapses than in controls (Supplementary Figure 2).

Altogether, these results indicate that ezrin ensures the appropriate topology and dynamics of signalling microclusters at the immunological synapse.

Ezrin silencing alters cell spreading and microtubule network organization at the immune synapse

The drastic differences in microcluster dynamics and localization in ezrin-silenced cells, without ezrin enrichment in microclusters, suggested to us that ezrin might have a function in the general organization of the immunological synapse. Indeed, T-cell spreading on stimulatory planar surfaces occurs through the generation of lamellipodia-like membrane extensions that structure immunological synapses (Dustin, 2008) and could be perturbed by ezrin silencing. We, therefore, investigated whether ezrin silencing could alter general features of the synapse, such as cell shape, as well as the organization of the cortical actin cytoskeleton and microtubules.

Once fully spread, most control cells (Jurkat and primary T cells) displayed approximate round shapes (Supplementary Figure 3A and B, left panels). In contrast, ezrin-silenced cells

spread to a certain extent, but formed less regular contact zones with multi-lobbed contours (Supplementary Figure 3A and B, right panels). Morphometric analyses showed that ezrin-silenced cells displayed lower shape factor values than control cells (Supplementary Figure 3C and D), indicating more irregular shapes.

Shape differences were not due to a general failure to structure the cortical actin cytoskeleton in lamellipodium-like membrane protrusions, as the presence of F-actin and moesin at the periphery of the synapse was not significantly affected by ezrin silencing (Supplementary Figure 4).

In *Drosophila*, the lack of moesin, the only ERM protein in this organism, lead to altered cell shape and impaired microtubule spindle organization during mitosis (Carreno *et al*, 2008; Kunda *et al*, 2008). We, therefore, hypothesized that ezrin silencing could affect microtubule organization at the synapse. Concomitantly with cell spreading, the microtubule-organizing centre (MTOC) was reoriented towards the contact zone. Moreover, in control Jurkat cells, microtubules formed a radial array initiated at the MTOC and surrounding the nucleus that then reached and stopped perpendicularly to the cell periphery (Figure 3A, arrowheads). SLP-76 microclusters were aligned on microtubules. In contrast, in ezrin-silenced cells, the radial array of microtubules appeared disorganized with microtubules bundles accumulated around the MTOC. More strikingly, fewer microtubules extended towards the cell periphery and when they did, they seemed tangled curving along the plasma membrane (Figure 3B, arrowheads). Similar results were found with a different siRNA ezrin oligonucleotide, ruling out off target effects (Figure 3C). To quantify microtubule alterations provoked by ezrin silencing, we assessed MTOC positioning towards the contact zone, which depends on the appropriate anchoring of microtubules to the periphery of the synapse (Kuhn and Poenie, 2002). Thus, ezrin-silenced cells, although frequently reoriented the MTOC towards the contact zone, as seen by epifluorescence microscopy, less efficiently apposed the MTOC to the stimulatory surface, as assessed by total internal reflection fluorescence (TIRF) microscopy (Figure 3D–F).

Consistent results were found with human primary CD4 T cells. Although less finely patterned than in Jurkat T cells, primary T cells displayed radial microtubules that reached the periphery of the contact zone in control cells, but much less efficiently in ezrin-silenced cells (Figure 3G and H).

To further assess the relationship between the persistence of microcluster aggregates and disordered microtubule network in ezrin-silenced cells, we analysed the effect of the microtubule polymerization inhibitor colchicine on microcluster distribution and dynamics. Interestingly, colchicine-treated cells displayed multi-lobbed shapes and SLP-76/pLAT microcluster aggregates (Figure 3I) resembling those of ezrin-silenced cells (Figures 2D, H and 3B). Moreover, SLP-76 microcluster dynamics in colchicine-treated cells displayed alterations similar to those found in ezrin-silenced cells (Figure 3J; Supplementary Movie 3).

Therefore, ezrin is required for microtubule network organization at the immunological synapse, which in turn ensures microcluster dynamics.

Ezrin silencing leads to enhanced TCR signalling
Given that ezrin silencing altered the topology and dynamics of several important signalling effectors at the immunological synapse, we investigated further its possible impact on TCR signalling. To this end, we analysed various early activation events in cells stimulated with sAg-pulsed APCs, soluble anti-CD3 or anti-CD3-coated coverslips.

Interestingly, the signalling capacity of ezrin-silenced cells was not impaired, but in all cases significantly enhanced. Thus, pTyr content at Jurkat/APC synapses was increased in ezrin-silenced cells (Figure 4B). Western blots revealed at least seven main hyper-phosphorylated polypeptides in ezrin-silenced cells (Figure 4C, arrows). In particular, the regulatory Tyr^{783} residue of phospholipase C (PLC)γ-1 was hyper-phosphorylated (Figure 4D). Higher pLAT content was also observed at the contact site of ezrin-silenced cells activated on anti-CD3-coated coverslips (Supplementary Figure 5). Finally, the activation of Erk1/2 serine-threonine kinases was also enhanced in ezrin-silenced cells activated with sAg-APCs, as assessed by the phosphorylation of Thr^{202}/Tyr^{204} regulatory residues (Figure 4E). Consistently, ezrin-silenced primary CD4 T cells stimulated with soluble anti-CD3 displayed enhanced pErk1/2 content, as assessed by intracellular FACS analysis (Figure 4G).

To better dissect the regulatory function of ezrin in TCR signalling, we monitored Erk1/2 activation kinetics. In the absence of co-stimulus, TCR engagement with an anti-CD3 mAb induced a fast activation phase followed by a de-activation phase that could be monitored by FACS analysis and characterized by the appearance of two cell populations of distinct pErk content. The whole cell population was fully activated within 3 min in both control and ezrin-silenced cells (Figure 5A), suggesting that ezrin silencing did not affect the activation phase. In contrast, when pErk fluorescence started to regress, distinct histogram profiles were observed in control and ezrin-silenced cells. In the latter, more cells displayed intermediate levels of Erk1/2 phosphorylation (Figure 5A, left versus right panels), indicating a slower de-activation phase. Interestingly, colchicine-treated cells also displayed a slower de-activation phase similar to that of ezrin-silenced cells (Figure 5B, left versus right panel).
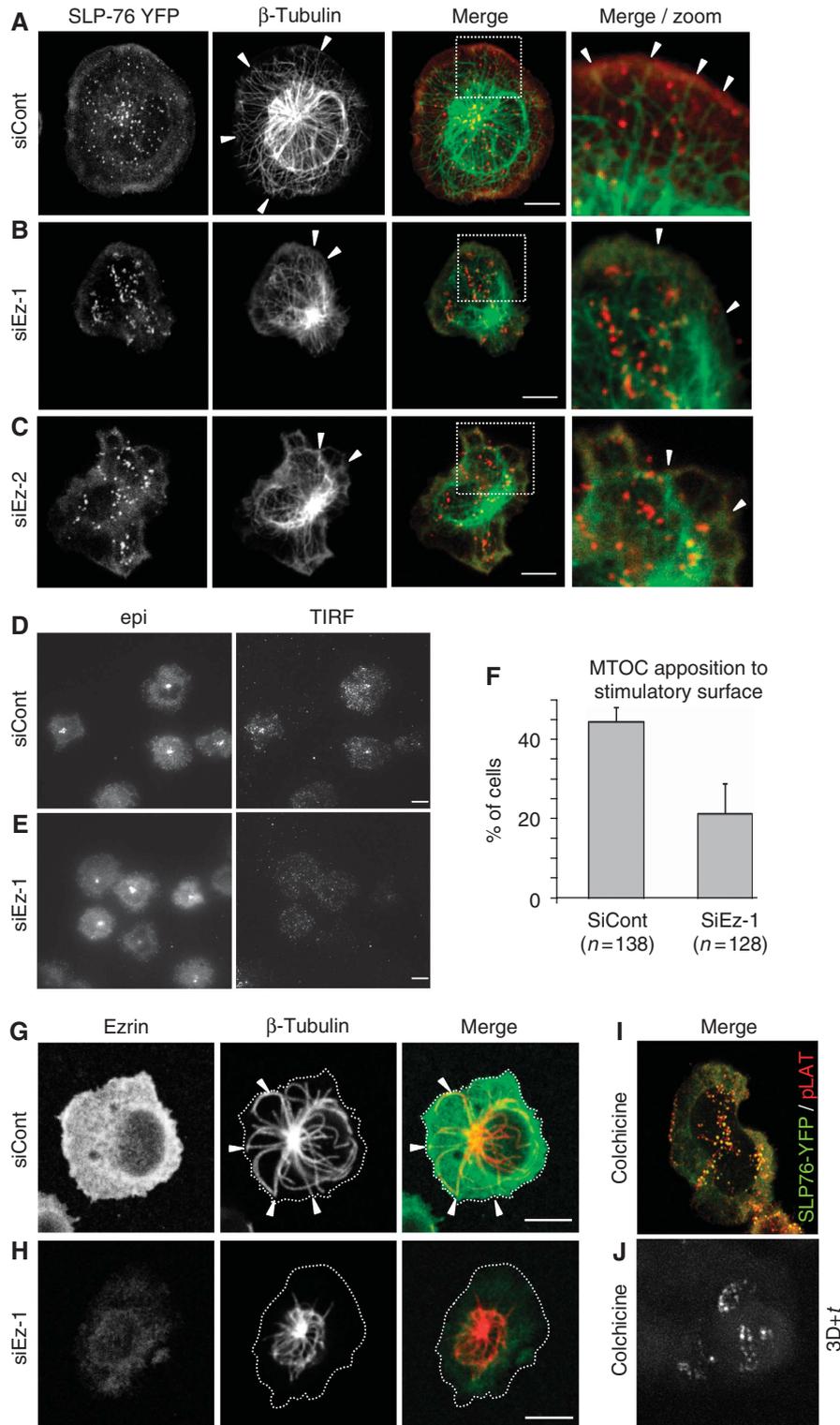
Altogether, these data indicate that ezrin controls microtubule network organization at the immunological synapse. Moreover, ezrin silencing leads to enhanced TCR-proximal signalling. On the basis of earlier studies linking microcluster centripetal movement to down-regulation of TCR signalling (Mossman *et al*, 2005; Varma *et al*, 2006), our results are consistent with a model in which the defects in microtubule-based microcluster centralization in ezrin-silenced T cells lead to an impaired negative regulation of TCR signalling.

The enhanced TCR signalling capacity of ezrin-silenced cells shown here seems in contradiction with earlier data showing that over-expression of the ezrin FERM domain, or the genetic inactivation of ezrin, lead to impaired NF-AT activation and IL2 production (Allenspach *et al*, 2001; Roumier *et al*, 2001; Shaffer *et al*, 2009). We, therefore, investigated the effect of ezrin silencing on NF-AT activation. In line with earlier findings, ezrin-silencing impaired NF-AT activation in response to sAg-pulsed APCs (Supplementary Figure 6). Interestingly, no significant alteration was found on NF-κB-mediated transcription and a weak inhibition was observed on AP-1-driven transcription. Noteworthy, we observed similar inhibitory effects of ezrin silencing in cells activated with calcium ionophore and phorbol ester

that bypass the TCR-proximal activation events. Similar results were obtained with an unrelated siRNA oligonucleotide, ruling out off target effects of the siRNA ezrin. Finally, a similar effect of ezrin silencing on NF-AT activation was observed using NF-AT-driven YFP expression as a read out (Supplementary Figure 6). Therefore, these data indicate that ezrin is necessary for NF-AT, but not NF-κB, activation.

Dlg1 links ezrin with microtubule organization at the synapse and with NF-AT activation

We next searched a molecular link explaining ezrin dual regulation of synapse architecture and NF-AT activation. Several evidences from different experimental systems pointed to the PDZ-domain-containing scaffold protein Dlg1. First, Dlg1 was shown to interact with ezrin FERM domain in epithelial cells (Lue *et al*, 1996); second, Dlg1 is

part of a molecular complex necessary for microtubule inter-action with the cell cortex and MTOC positioning in migrating astrocytes (Etienne-Manneville *et al*, 2005); third, Dlg1 trans-locates to the immunological synapse and regulates T-cell activation (Xavier *et al*, 2004; Round *et al*, 2005) and fourth, Dlg1 regulates NF-AT activation without affecting NF-κB (Round *et al*, 2007). We, therefore, looked for a functional relationship between ezrin and Dlg1.

First, consistent with the reported ezrin–Dlg1 interaction in epithelial cells (Lue *et al*, 1996), we found that Dlg1 was enriched together with ezrin at the periphery of the immu-nological synapse (Figure 6A, arrowheads). Moreover, ezrin silencing delocalized Dlg1 from this zone of the synapse (Figure 6B and C). Finally, we found, using the proximity ligation *in situ* assay (Duolink) (Fredriksson *et al*, 2002; Soderberg *et al*, 2006; Infantino *et al*, 2010), that Dlg1 inter-acted with ezrin in T cells, but not with moesin. Interaction seemed constitutive as it was detected in non-activated cells and did not increase with activation (Figure 6D–G). In cells spread on anti-CD3, spots of Dlg1–ezrin interaction were detected mainly in the lamellipodium-like membrane exten-sions, more concentrated, though not uniquely present, in the peripheral zone (Figure 6F and G). Similar results were obtained in primary T cells (Figure 6H and I). Second, similarly to ezrin, Dlg1 silencing (Figure 7B) perturbed cell shape, microcluster topology, microtubule network organiza-tion at the synapse and MTOC positioning (Figure 7A, C and D). Alterations of microtubule patterns were also found in primary CD4 T cells (Figure 7E–G). Third, Dlg1 silencing lead to enhanced Erk1/2 activation (Figure 7H).

The inhibitory effect of ezrin silencing on NF-AT activation, without affecting NF-κB (Supplementary Figure 6) resembled that of Dlg1, which was shown to regulate NF-AT activation through the p38 MAP kinase alternative activation pathway (Round *et al*, 2007). In line with these observations, we found that ezrin silencing lead to an inhibition of p38 activation, although to a lesser extent than Dlg1 silencing (Figure 7I and J).

Altogether, these data indicate that ezrin and Dlg1 act together to regulate immune synapse architecture and to dually control Erk1/2 and NF-AT activation.

Discussion

The data we report here are consistent with a model in which ezrin cooperates with Dlg1 to control immune synapse archi-tecture and T-cell activation. First, ezrin and Dlg1 would set the microtubule architecture at the synapse, which in turn would be necessary to drive signalling microcluster dynamics and the down-regulation of TCR-proximal signalling. Second, the correlative data between ezrin and Dlg1-silencing effects shown here, together with those reported by Round *et al* (2007), are highly suggestive of a causal connection between ezrin and Dlg1 in regulating NF-AT activation through p38 MAP kinase.

The topology and movement of signalling microclusters at the immunological synapse are important for triggering and controlling TCR signal transduction (Mossman *et al*, 2005; Varma *et al*, 2006). On the basis of the localization of phosphorylated signalling molecules, such as Lck, ZAP-70, LAT and SLP-76, it was proposed that TCR signalling was first taking place at the initial sites of contact between T cells and APCs, and then, during a second phase of microcluster nucleation, at the periphery of the immunological synapse. Then, microclusters containing signalling molecules move towards the centre of the synapse in which signal extinction was proposed to take place (Bunnell *et al*, 2002; Mossman *et al*, 2005; Yokosuka *et al*, 2005; Barr *et al*, 2006; Varma *et al*, 2006; Cemerski *et al*, 2008; Nguyen *et al*, 2008). The segrega-tion into central and peripheral supramolecular activation clusters during immune synapse formation seemed to sepa-rate activation and de-activation processes tuning TCR signal-ling (Varma *et al*, 2006; Cemerski *et al*, 2008; Yokosuka *et al*, 2008). However, how immune synapse architecture is orga-nized and influences TCR signalling remained elusive.

We show that ezrin and Dlg1 are necessary for the posi-tioning of microtubules at the periphery of the immunological synapse, which likely conditions MTOC polarization. These findings are in line with earlier reports showing that the depletion of moesin, the only ERM family member expressed in *Drosophila*, lead to alterations in microtubule organization, compromising spindle positioning during mitosis (Carreno *et al*, 2008; Kunda *et al*, 2008). They are also in line with reports showing an important function of Dlg1 in MTOC positioning during astrocyte migration (Etienne-Manneville *et al*, 2005).

Structured microtubule networks in the synapse appear, in turn, required for the engagement of microclusters into centripetal movements that likely bring them to zones of signal extinction. Consistently, colchicine-treated and ezrin-silenced cells behaved similarly with regard to microcluster patterning, microcluster dynamics and Erk1/2 de-activation mode. It was earlier reported that the generation of peripheral microclusters and their movement within the immunological

Figure 3 Ezrin silencing impairs the microtubule network organization at the synapse. (**A–C**) Jurkat J14 cells expressing YFP-SLP-76, transfected with siRNA control or siRNA ezrin (two different oligonucleotides, siEz-1 and siEz-2), were activated for 3 min on coverslips coated with anti-CD3 mAb, fixed, stained with anti-β-tubulin Ab and analysed by confocal microscopy. Arrowheads show the peripheral zone of the immunological synapse in which thin microtubule structures reach the cell cortex. Right panels zoom the area marked by a frame in the merge image. An optical section at the contact surface is shown. (**D, E**) Jurkat J77 cells transfected with siRNA control or siRNA ezrin-1 were activated on anti-CD3-coated coverslips for 3 min and fixed. MTOC was stained with anti-centrin Ab and observed by epifluorescence ('epi') or TIRF microscopy. (**F**) Percentage of cells with MTOC apposed to the contact surface (detected by TIRF microscopy). The plot shows pooled data from three independent experiments ± s.d. (**G, H**) Primary CD4 T cells transfected with siRNA control or siRNA ezrin-1 were activated 5 min on anti-CD3 + anti-CD28-coated coverslips, fixed and stained for ezrin and for β-tubulin. Cell edges are marked by a dotted line. Arrowheads show areas in which microtubules seem to reach the periphery of the immune synapse. In ezrin-silenced cells, microtubules reach much less frequently the periphery of the immune synapse staying in a smaller zone. A single optical section at the level of the contact surface is shown. (**I**) Jurkat J14 cells expressing YFP-SLP-76 were treated with 2 μM colchicine for 30 min, activated 3 min on anti-CD3-coated coverslips, fixed, stained with anti-pLAT Ab and analysed by confocal microscopy. An optical section at the contact surface is shown. A representative experiment out of three is shown. Scale bar = 5 μm. (**J**) Jurkat J14 cells expressing YFP-SLP-76 were treated with 5 μM colchicine for 30 min, activated on anti-CD3-coated coverslips and subjected to live cell imaging. The picture shows 3D + time projections of YFP-SLP-76 microclusters recorded during 5 min at 6 images/min (Supplementary Movie 3).
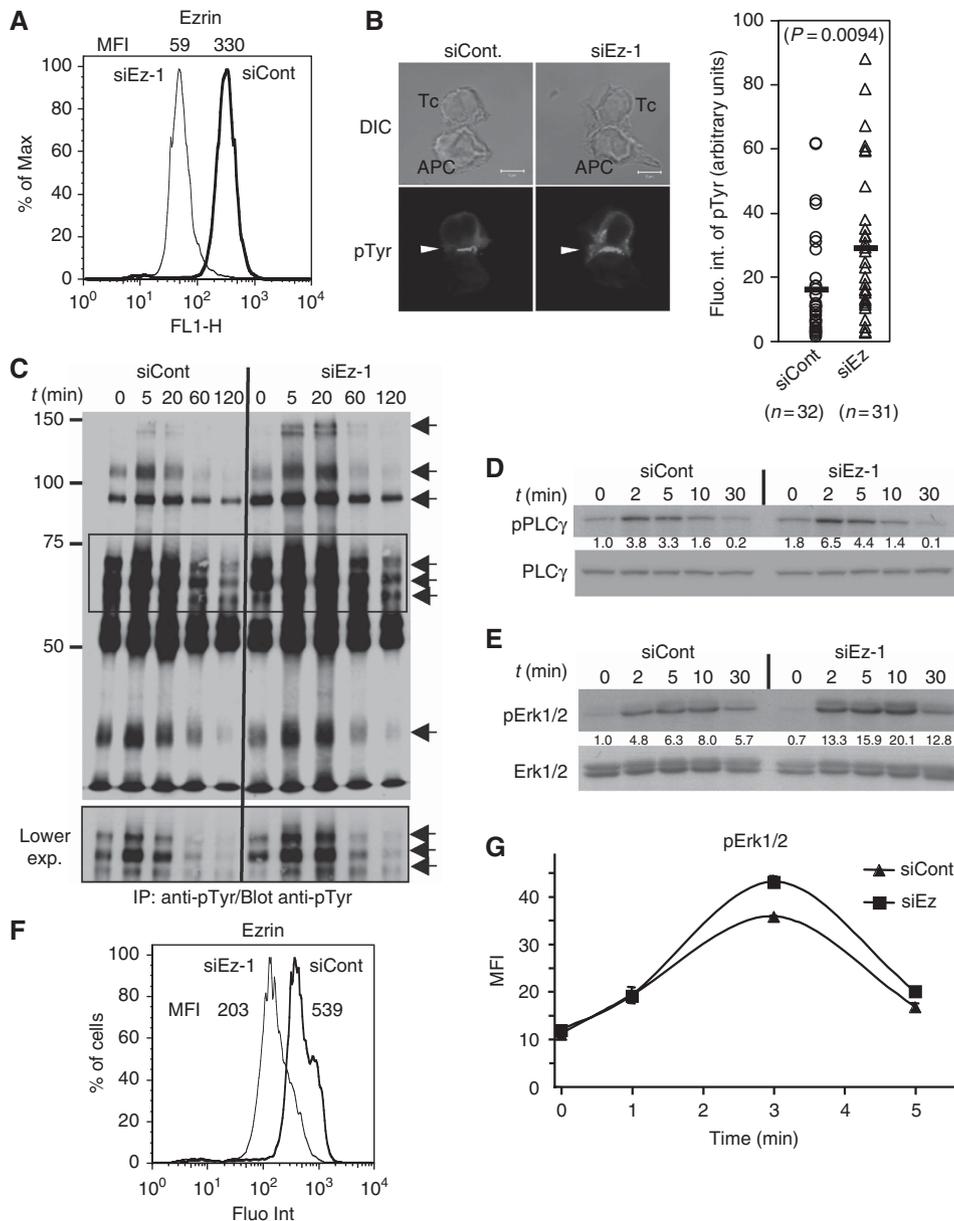
Figure 4 Ezrin silencing leads to enhanced TCR-proximal signalling. (**A–E**) Jurkat J77 cells transfected with siRNA control or siRNA ezrin-1 were processed as follows: (**A**) Cells were fixed, stained with anti-ezrin Abs and analysed by flow cytometry. Mean fluorescence intensity of the peaks (MFI) is indicated above. Ezrin expression in ezrin-silenced cells was reduced by 80%. (**B**) Cells were activated with sAg-pulsed Raji cells for 20 min, set on coverslips, fixed and stained with anti-pTyr mAb (left). Fluorescence intensity of pTyr at the synapse was analysed by quantitative image analysis (right). (**C**) Cells were activated with sAg-pulsed Raji cells for 5, 20, 60 and 120 min. Cell lysates were immunoprecipitated with anti-pTyr mAb, and analysed by western blot using the same Ab. Arrows show major tyrosine phosphorylated polypeptides. The middle part of the blot (framed) is shown at a lower exposure in the lower panel. (**D, E**) Cells were activated with sAg-pulsed Raji cells for 2, 5, 10 and 30 min. Total cell lysates were analysed by western blot using Abs against the activatory tyrosine residue pTyr[783] of PLCγ-1 (**D**, upper panel) and further revealed with anti-PLCγ-1 (**D**, lower panel). Alternatively, western blots were revealed with Abs directed to the activatory residues (Thr[202]/Tyr[204]) of Erk1/2 (**E**, upper panel) and further revealed with anti-Erk1/2 (**E**, lower panel). The density of bands corresponding to pPLCγ1 or pErk were normalized with respect to the amount of PLCγ1 or total Erk per lane, and then normalized to intensity of siCont at $t = 0$. Values are indicated between the two blots. (**F, G**) Primary CD4 T cells transfected with siRNA control, or siRNA ezrin-1 were activated with soluble anti-CD3 Ab (MEM92) for the indicated times, fixed and stained with anti-ezrin (**F**) and pErk (**G**) Abs and analysed by flow cytometry. Mean fluorescent intensity of anti-ezrin staining is shown on the side of the histograms (**F**). Ezrin expression in ezrin-silenced cells was reduced by 60%. Mean fluorescence intensity of triplicates ± s.d. of anti-pErk is plotted versus time. Note that s.d. bars in the curve points in (**G**) are small and hidden by the curve symbols. A representative experiment out of three independent experiments is shown.

synapse was dependent on actin and myosin-II dynamics (Campi *et al*, 2005; Varma *et al*, 2006; Nguyen *et al*, 2008; Ilani *et al*, 2009). Ezrin silencing did not perturb F-actin and moesin localization at the periphery of the synapse, suggesting that the cortical actin cytoskeleton was not largely altered.

Actin and microtubule dynamics might cooperate to structure immunological synapses and to drive, perhaps sequentially, microcluster centripetal movements.

Our observations are consistent with a model in which ezrin would interact with the cortical actin cytoskeleton
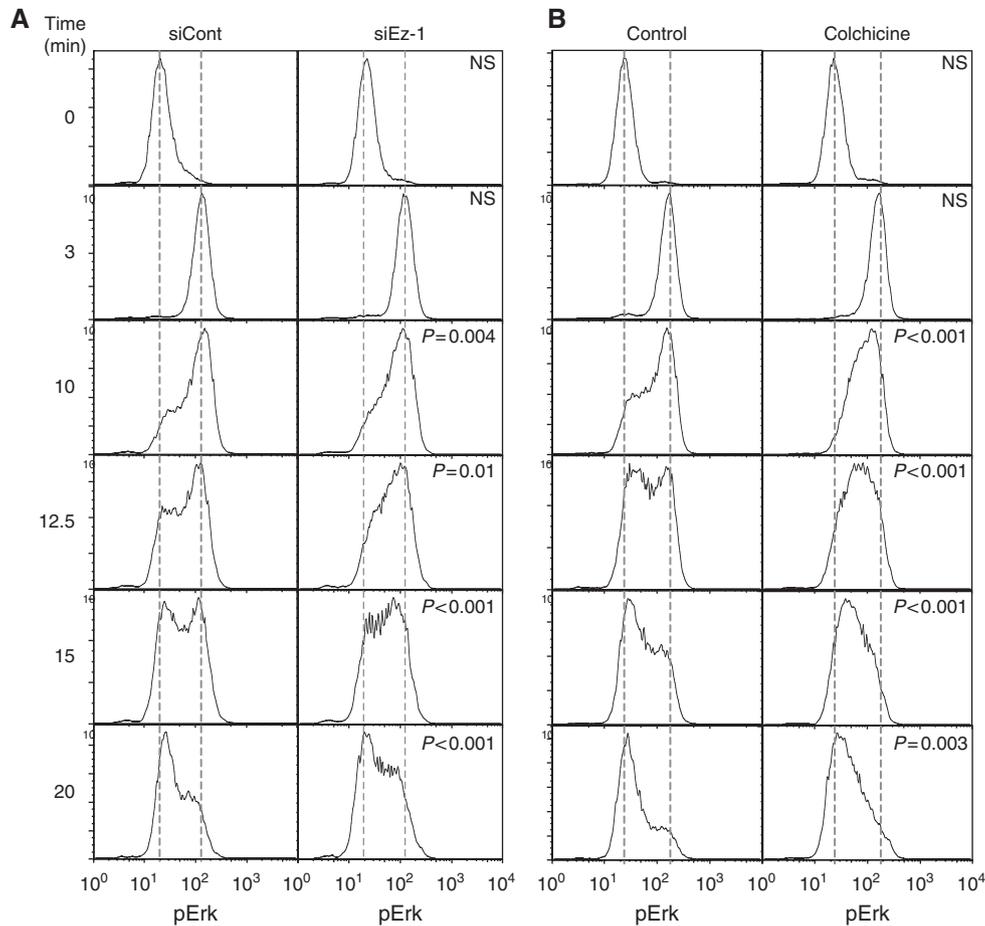
Figure 5 Erk1/2 de-activation kinetics are altered in ezrin-silenced cells. (**A**) Jurkat J77 cells transfected with siRNA control, or siRNA ezrin-1 were activated with soluble anti-CD3 Ab (MEM92) for the indicated times. Cells were then fixed, permeabilized, stained with anti-pErk1/2 Ab and analysed by flow cytometry. (**B**) Jurkat J77 cells were treated with 2 μg/ml of colchicine for 30 min, then activated and processed as in (**A**). Histograms represent fluorescence intensity of pErk versus number of cells. Graphs were rescaled to have the peaks at the same height using FlowJo software, to facilitate the comparison of curve shapes. The significance of the differences in cell distribution between activated and non-activated populations was calculated by comparing curve shapes as described in Supplementary data. '*P*'-value is indicated in each panel. Dashed lines mark the mean fluorescence intensity values of unstimulated or maximally activated control cells. The figure shows a representative experiment out of three independent experiments carried out. NS = non-significant.

through its C-terminal domain (Fievet *et al*, 2007) and with Dlg1, through its FERM domain (Lue *et al*, 1996). Dlg1, in turn, would facilitate the interaction of microtubules with the cell cortex at the periphery of the synapse through a complex mechanism involving other cell polarity regulators (Etienne-Manneville *et al*, 2005). In addition, ezrin and Dlg1 may interact with TCR signalling effectors (Xavier *et al*, 2004; Round *et al*, 2005; Ilani *et al*, 2007), but the function of this interaction in microcluster nucleation or dynamics remains unclear. By acting on both microtubule architecture and the localization of signalling molecules, ezrin and Dlg1 might help to establish the second phase of microclusters generation after T-cell spreading during which microclusters are formed at the periphery of the synapse and then move towards the centre of the synapse.

Ezrin silencing resulted in enhanced tyrosine phosphorylation of various substrates, as well as Erk1/2 activation. Consistently, we did not observe any negative effects on conjugate formation (data not shown). This was in agreement with earlier reports by others and us that showed no impairment of conjugate formation in cells over-expressing the ezrin FERM domain (Roumier *et al*, 2001; Faure *et al*,

2004), or in T cells from ezrin-deficient mice (Shaffer *et al*, 2009). In contrast, Ilani *et al* (2007) showed that over-expression of ezrin mutants T^{235}T^{567}/AA or EE inhibited conjugate formation and ZAP-70 relocalization to anti-CD3/28-coupled beads. These discrepancies may be due to the procedures used to perturb ezrin function. Moreover, Shaffer *et al* (2009) showed unchanged, or increased, Erk1/2 activation in T cells from ezrin-deficient mice activated with anti-CD3 Abs. We consistently found enhanced Erk1/2 activation in Jurkat and primary human T cells treated with siRNA ezrin, either activated with sAg-pulsed B cells, or with anti-CD3 Abs. The enhanced Erk1/2 phosphorylation in ezrin-silenced cells could be explained by the fact that ezrin silencing seemed not to affect the triggering phase of early signalling, but rather a negative feedback loop that rapidly controls the extent of TCR-proximal signalling. Therefore, the architecture of the immunological synapse, and the appropriate topology and microtubule-dependent movement of microclusters are important for the negative control of TCR-proximal signalling, rather than for TCR triggering, which occurs anyway in the absence of ezrin and microtubules.
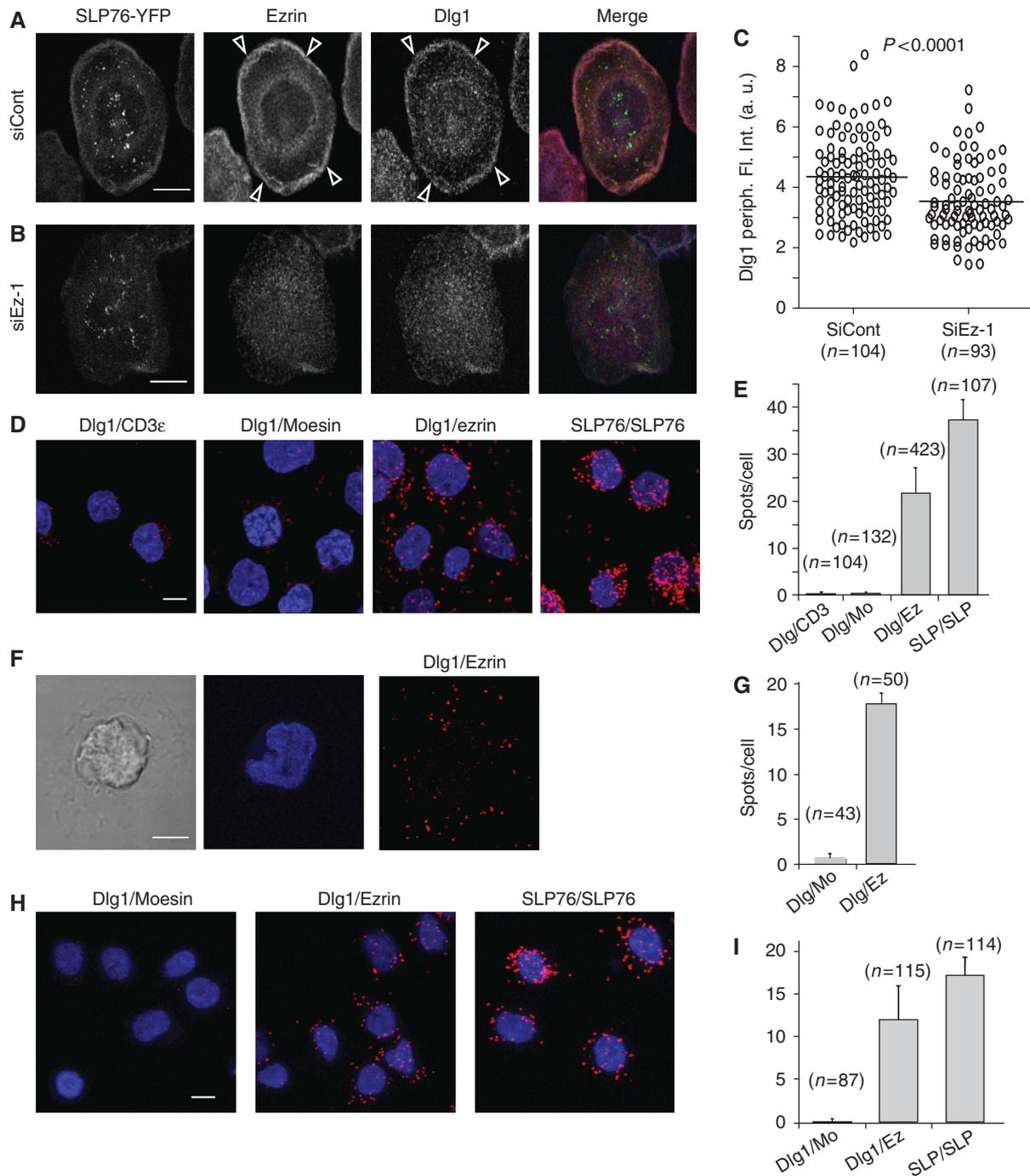
Figure 6 Ezrin interacts with Dlg1. (**A**, **B**) Jurkat J14 cells expressing YFP-SLP-76, transfected with siRNA control or siRNA ezrin-1, were activated 3 min on anti-CD3-coated coverslips, fixed, stained with anti-ezrin and anti-Dlg1 Abs and analysed by confocal microscopy. A confocal section at the contact surface is shown. Arrowheads point to the peripheral zone in which ezrin and Dlg1 are enriched. (**C**) Fluorescence intensity corresponding to Dlg1 staining at the periphery of the immunological synapse was quantified automatically as described in Materials and methods. (**D**) Jurkat J77 cells were adhered to poly-L-lysine coverslips, fixed and stained with pairs of antibodies as depicted in the figure: Dlg1-CD3ε (negative control), Dlg1-moesin, Dlg1-ezrin and two anti-SLP-76 Abs (positive control). The putative interaction of the molecules stained with each pair of Abs was then assessed using Duolink technology, as described in Materials and methods. Spots show molecular proximity and are indicative of molecular interactions. (**F**) Jurkat J77 cells were activated for 3 min on anti-CD3-coated coverslips. The interaction between Dlg1 and ezrin was assessed by Duolink and quantified as above (**G**). Moesin labelling was here the negative control. (**H**) Primary CD4 T cells adhered to poly-L-lysine coverslips, fixed and stained with pairs of antibodies as depicted in the figure: Dlg1-moesin, Dlg1-ezrin and two anti-SLP-76 Abs (positive control). (**E**, **G**, **I**) The spots per cell were automatically counted using BlobFinder software. Average values of number of spots/cell in different microscopy fields ± s.d. is plotted. The number of cells analysed per condition is shown in parenthesis. One representative experiment is shown out of three carried out for (**A–E**) and of two for (**F–I**). Scale bar = 5 μm.

In spite of the enhanced early signalling capacities of ezrin-silenced cells, NF-AT activation was strongly inhibited, in line with earlier observations (Sperling *et al*, 1998; Roumier *et al*, 2001; Shaffer *et al*, 2009). Interestingly, AP-1 and NF-κB-driven transcription were mildly inhibited or unaltered by ezrin silencing, respectively. This was reminiscent of the
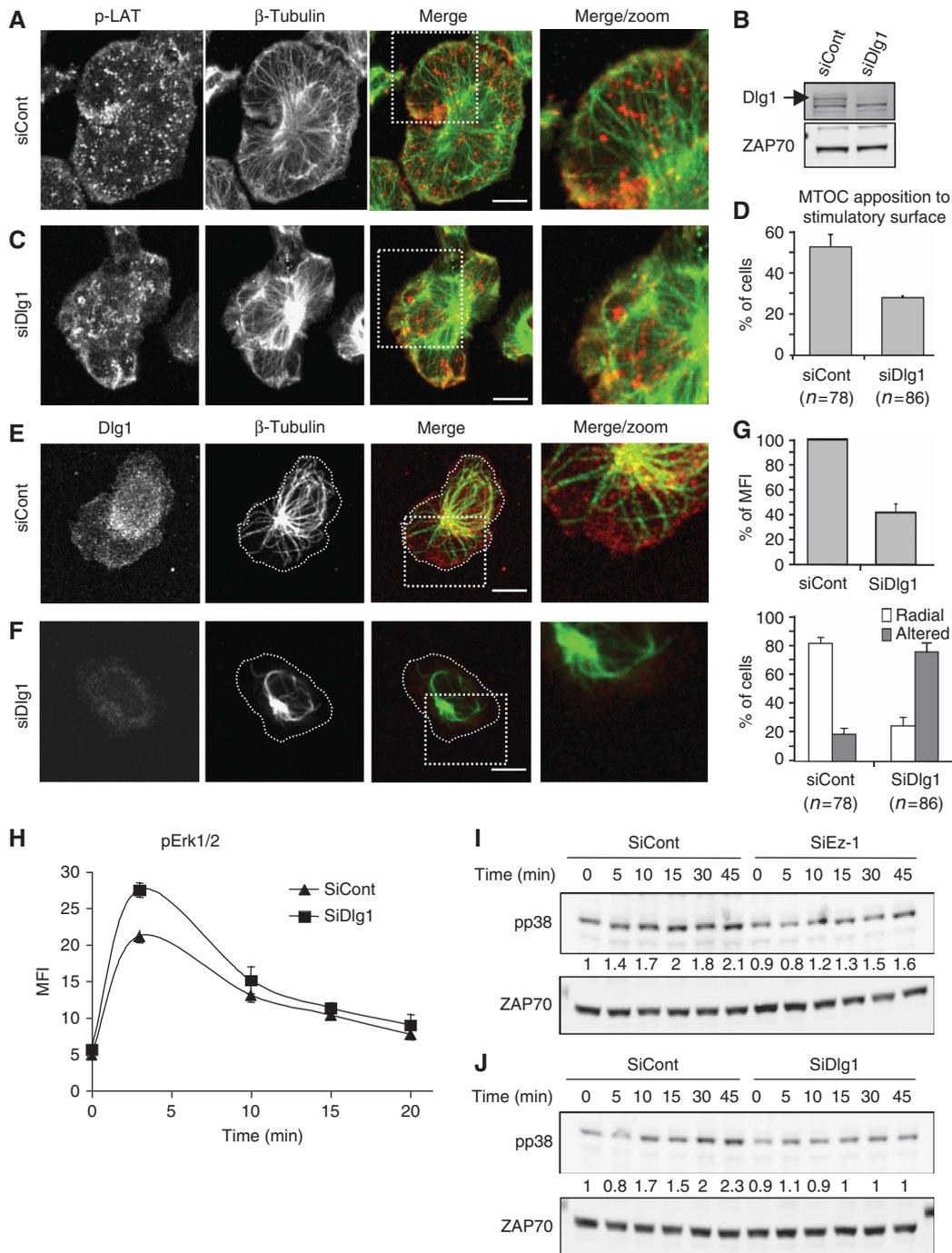
Figure 7 Dlg1 links ezrin with microtubule organization at the synapse and with p38 MAP kinase activation. (**A, C**) Jurkat J14 cells expressing YFP-SLP-76, transfected with siRNA control or siRNA Dlg1, were activated for 3 min on anti-CD3-coated coverslips, fixed and stained with anti-β-tubulin and anti-pLAT. Right panels show an enlargement of the framed zone in merge panels. A single optical section of the contact surface is shown. Scale bar = 5 μm. (**B**) Cell lysates from Jurkat J77 cells transfected with siRNA control, or siRNA Dlg1 were analysed by western blot using anti-Dlg1 Ab. The inhibition of Dlg1 expression in siRNA Dlg1-transfected cells was ∼ 85%. (**D**) Jurkat J77 cells transfected with siRNA control, or siRNA Dlg1 were activated for 3 min on anti-CD3-coated coverslips, fixed, stained with anti-centrin Ab and analysed by epifluorescence or TIRF microscopy as in Figure 3C and D. The percentage of cells displaying the MTOC apposed to the stimulatory surface detected by TIRF is shown. Pooled data from two independent experiments ± s.d. are shown. (**E, F**) Primary CD4 T cells were transfected with siRNA control or siRNA Dlg1, activated for 5 min on anti-CD3 + CD28-coated coverslips, fixed and stained with anti-β-tubulin and anti-Dlg1. Right panels show an enlargement of the framed zone in merge panels. A single optical section of the contact surface is shown. Scale bar = 5 μm. (**G**) Upper histogram: quantification by confocal microscopy of Dlg1 silencing in primary CD4 T cells ± s.d. Lower histogram: the percentage of primary CD4 T cells displaying radial microtubules reaching the cells extensions (i.e. panel **E**), or displaying altered, non-radial microtubules (i.e. panel **F**) were scored by visual counting. Pooled data from three independent experiments ± s.d. are shown. (**H**) Jurkat J77 cells transfected with siRNA control, or siRNA Dlg1 were activated with soluble anti-CD3 Ab (MEM92) for the indicated times. Cells were then fixed, permeabilized, stained with anti-pErk1/2 Abs and analysed by flow cytometry. The average of duplicates ± s.d. of mean fluorescence intensity versus time is shown. A representative experiment out of three performed is shown. (**I, J**) Jurkat J77 cells transfected with siRNA control, siRNA ezrin (**I**), or siRNA Dlg1 (**J**) were activated with sAg-pulsed Raji cells for 5, 10, 15, 30 and 45 min. Total lysates were analysed by western blot using Abs directed to the phosphorylated activatory residues Thr^{180}/Tyr^{182} of p38 MAP kinase (upper panels) and further revealed with anti-ZAP-70 (lower panels). The intensity of bands corresponding to pp38 was normalized with respect to the amount of ZAP-70 per lane and then normalized to the intensity of bands of control cells at $t = 0$. Values are indicated between the blots. Representative experiment out of three performed.

reported effect of Dlg1 silencing on NF-AT activation, which was shown to occur through Dlg1 interaction with p38 MAP kinase and the regulation of the alternative pathway of activation of this kinase (Round *et al*, 2007). Consistent with a common mechanism, ezrin silencing also inhibited p38 activation. Importantly, ezrin silencing also inhibited NF-AT activation in cells activated with calcium ionophore and phorphol ester, suggesting that ezrin requirement for NF-AT activation was independent of TCR-proximal signalling.

In conclusion, our study underscores the importance of functional links between microtubules, the cortical actin cytoskeleton and cell polarity regulators in ensuring the architecture and function of immunological synapses. More importantly, our data highlight the significance of synapse architecture in the negative control of TCR signalling. Finally, our work reveals that ezrin and Dlg1 may balance T-cell activation events leading to Erk1/2 and NF-AT activation.

Materials and methods

See also Supplementary data.

Cells

The human leukaemia T-cell line Jurkat, clone J77cl20, and the APC Raji have been described (Roumier *et al*, 2001), as well as the SLP-76-deficient Jurkat derivative J14 (Yablonski *et al*, 1998). J14 cells were transfected with SLP-76-YFP expression constructs and stable cell clones selected using G418. CD4 T cells from peripheral blood of healthy donors were isolated and cultured as described (Hung *et al*, 2007).

Signalling microcluster experiments

SLP-76 microcluster dynamics was studied as described (Nguyen *et al*, 2008). Briefly, SLP-76-defective Jurkat cells (J14) stably expressing YFP-SLP-76 were transfected with siRNA control or siRNA ezrin oligonucleotides. Three days later, cells were resuspended at 2×10^6 cells/ml in non-fluorescent medium, dropped onto glass coverslips (MatTek or LabTek) coated with anti-CD3 mAb, UCHT-1 or MEM-92 when subsequent labelling using anti-IgG1 antibodies was necessary or anti-CD3 mAb + anti-CD28 for human CD4 primary T cells. Cells were imaged at 37°C under a spinning disk confocal microscope (Perkin Elmer Ultraview), equipped with stage and objective heater and CO_2 incubator. Z-stacks of 11 confocal sections were acquired every 5 s, during 5 min. Alternatively, cells were fixed at the indicated times, permeabilized and stained with the appropriate Abs. Cells were then analysed using a confocal microscope (Zeiss LSM510 or Leica SP5), or by total internal reflection fluorescence microscopy (Olympus). Fluorescence quantification and morphometric analyses were carried out using Metamorph software. Image deconvolution was performed with Huygens software.

Quantitative image analysis of microcluster aggregation

To locate accurately fluorescent spots, we have applied a wavelet filtering technique able to cancel background influence and enhance spots with a given size range (Olivo-Marin, 2002). In this image, each local maximum of intensity has been considered as a particle of interest when its intensity was above a statistical threshold, which allows the most accurate automatic detection of microclusters. From the positions of detected spots, we have extracted the relevant aggregates by the use of a statistical test on particle density in a local neighbourhood. In each image a density of particles d_0 is computed as the total number of detected spots divided by the area of the cell. Then for each pixel we have computed the likelihood of observing the actual number: m and of detected particles in a local neighbourhood: w. The latter is defined as a disk with a diameter of the typical size of an aggregate. The likelihood is the probability of observing m spots or more in w under the assumption of uniformly distributed particles with density d_0. When this probability is under 5%, we reject the assumption of uniformly distributed particles in the region w and deduce the presence of an aggregate of spots. This gives the rate of

aggregation for each cell, which is the number of spots belonging to an aggregate over the overall number of spots.

Conjugate formation, immunofluorescence staining and confocal microscopy

Jurkat cells were transfected twice with siCont and siEz oligonucleotides. Two days later, they were incubated for the indicated times at 37°C with APCs (Raji) unpulsed or pulsed with 10 μg/ml *Staphylococcus* enterotoxin E superantigen. Cells were then plated onto poly-L-lysine-coated coverslips, fixed with 4% paraformaldehyde for 20 min at room temperature. The fixed cells were then washed for 10 min with 50 mM NH4Cl in PBS, then once in PBS alone. Before staining, non-specific protein binding was blocked by incubating the coverslips for 15 min in 5% FCS 0.05% saponin in PBS. This buffer was used as washing and staining buffer for all the subsequent steps. Cells were then stained with the indicated primary antibody, washed, stained with the appropriate fluorescent-coupled secondary Ab and washed. Confocal microscopy analyses were carried on in a Zeiss LSM-510 or in a Leica SP5 confocal microscope. Quantitative image analyses of phospho-Tyr accumulation at the immunological synapse were performed using Meta-morph software (Universal Imaging) as described (Thoulouze *et al*, 2006). Three-dimensional reconstruction of immunological synapses was performed using Imaris software on images treated by deconvolution using Huygens software.

T-cell activation and intracellular FACs analysis

Cells were activated with soluble anti-CD3 (MEM92, 10 μg/ml) for various times. Cells were then fixed with 4% paraformaldehyde for 10 min at room temperature, washed twice in PBS alone and then permeabilized in 2% FCS, 0.1% saponin in PBS for 10 min. This buffer was also used for all the subsequent steps. Cells were then stained with the indicated primary antibody, washed, stained with the appropriate fluorescently tagged secondary Ab and washed. Samples were acquired using a FACsCalibur (BD) and analysed using FlowJo (Tree Star).

Quantitative image analysis of F-actin, moesin or Dlg1 enrichment at the periphery of the immunological synapse

Images used were a 2.5 μm projection of confocal optical sections at the contact surface of T cells activated for 3 min on anti-CD3-coated coverslips. Automatic quantification of F-actin, moesin, or Dlg1 fluorescence intensity at the periphery of the contact zone between T cells and anti-CD3-coated coverslips was performed using Acapella Image Analysis software (PerkinElmer). Briefly, cell border detection was obtained using membrane labelling with Cholera Toxin Alexa[488] or phalloidin labelling. From this border inside the cell, a ring region of 2 μm width was created. Fluorescence intensity corresponding to F-actin, moesin or Dlg1 labelling obtained with phalloidin, anti-moesin or anti-Dlg1 Abs, respectively, was then measured in this region. We considered this region as the periphery of the immunological synapse.

Proximity ligation in situ assay (Duolink[TM])

Interactions between ezrin and Dlg1 in T cells were analysed using the Duolink[TM] proximity ligation *in situ* assay (Fredriksson *et al*, 2002; Soderberg *et al*, 2006), according to manufacturer's instructions. Anti-Dlg1 rabbit polyclonal Ab was combined with anti-ezrin mouse mAb, anti-moesin mouse mAb or anti-CD3ε mouse mAb (negative control). The positive control was obtained using a combination of two anti-SLP-76 mouse mAb and rabbit polyclonal Ab. Fluorescence spots generated were automatically counted and the average number of spots per cell calculated from nuclei counting using BlobFinder software (Uppsala University).

Statistical analyses

They were performed by the Mann–Whitney non-parametric test using Prism software (Graphpad). FACS profile comparisons in Figure 5 were performed using a Bootstrap test (Supplementary data).

Supplementary data

Supplementary data are available at *The EMBO Journal* Online (http://www.embojournal.org).

Acknowledgements

Conflict of interest

The authors declare that they have no conflict of interest.

References

Acuto O, Di Bartolo V, Michel F (2008) Tailoring T-cell receptor signals by proximal negative feedback mechanisms. *Nat Rev Immunol* **8:** 699–712

Allenspach EJ, Cullinan P, Tong J, Tang Q, Tesciuba AG, Cannon JL, Takahashi SM, Morgan R, Burkhardt JK, Sperling AI (2001) ERM-dependent movement of CD43 defines a novel protein complex distal to the immunological synapse. *Immunity* **15:** 739–750

Barr VA, Balagopalan L, Barda-Saad M, Polishchuk R, Boukari H, Bunnell SC, Bernot KM, Toda Y, Nossal R, Samelson LE (2006) T-cell antigen receptor-induced signaling complexes: internalization via a cholesterol-dependent endocytic pathway. *Traffic* **7:** 1143–1162

Bunnell SC, Hong DI, Kardon JR, Yamazaki T, McGlade CJ, Barr VA, Samelson LE (2002) T cell receptor ligation induces the formation of dynamically regulated signaling assemblies. *J Cell Biol* **158:** 1263–1275

Burkhardt JK, Carrizosa E, Shaffer MH (2008) The actin cytoskeleton in T cell activation. *Annu Rev Immunol* **26:** 233–259

Campi G, Varma R, Dustin ML (2005) Actin and agonist MHC-peptide complex-dependent T cell receptor microclusters as scaffolds for signaling. *J Exp Med* **202:** 1031–1036

Carreno S, Kouranti I, Glusman ES, Fuller MT, Echard A, Payre F (2008) Moesin and its activating kinase Slik are required for cortical stability and microtubule organization in mitotic cells. *J Cell Biol* **180:** 739–746

Cemerski S, Das J, Giurisato E, Markiewicz MA, Allen PM, Chakraborty AK, Shaw AS (2008) The balance between T cell receptor signaling and degradation at the center of the immunological synapse is determined by antigen quality. *Immunity* **29:** 414–422

Charrin S, Alcover A (2006) Role of ERM (ezrin-radixin-moesin) proteins in T lymphocyte polarization, immune synapse formation and in T cell receptor-mediated signaling. *Front Biosc* **11:** 1987–1997

D'Angelo R, Aresta S, Blangy A, Del Maestro L, Louvard D, Arpin M (2007) Interaction of ezrin with the novel guanine nucleotide exchange factor PLEKHG6 promotes RhoG-dependent apical cytoskeleton rearrangements in epithelial cells. *Mol Biol Cell* **18:** 4780–4793

Delon J, Kaibuchi K, Germain RN (2001) Exclusion of CD43 from the immunological synapse is mediated by phosphorylation-regulated relocation of the cytoskeletal adaptor moesin. *Immunity* **15:** 691–701

Dustin ML (2008) T-cell activation through immunological synapses and kinapses. *Immunol Rev* **221:** 77–89

Etienne-Manneville S, Manneville JB, Nicholls S, Ferenczi MA, Hall A (2005) Cdc42 and Par6-PKCzeta regulate the spatially localized association of Dlg1 and APC to control cell polarization. *J Cell Biol* **170:** 895–901

Faure S, Salazar-Fontana LI, Semichon M, Tybulewicz VLJ, Bismuth G, Trautmann A, Germain RN, Delon J (2004) ERM proteins regulate cytoskeleton relaxation promoting T cell-APC conjugation. *Nat Immunol* **5:** 272–279

Fehon RG, McClatchey AI, Bretscher A (2010) Organizing the cell cortex: the role of ERM proteins. *Nat Rev Mol Cell Biol* **11:** 276–287

Fievet B, Louvard D, Arpin M (2007) ERM proteins in epithelial cell organization and functions. *Biochim Biophys Acta* **1773:** 653–660

Fievet BT, Gautreau A, Roy C, Del Maestro L, Mangeat P, Louvard D, Arpin M (2004) Phosphoinositide binding and phosphorylation act sequentially in the activation mechanism of ezrin. *J Cell Biol* **164:** 653–659

Fredriksson S, Gullberg M, Jarvius J, Olsson C, Pietras K, Gustafsdottir SM, Ostman A, Landegren U (2002) Protein detection using proximity-dependent DNA ligation assays. *Nat Biotechnol* **20:** 473–477

Hung CH, Thomas L, Ruby CE, Atkins KM, Morris NP, Knight ZA, Scholz I, Barklis E, Weinberg AD, Shokat KM, Thomas G (2007) HIV-1 Nef assembles a Src family kinase-ZAP-70/Syk-PI3K cascade to downregulate cell-surface MHC-I. *Cell Host Microbe* **1:** 121–133

Ilani T, Khanna C, Zhou M, Veenstra TD, Bretscher A (2007) Immune synapse formation requires ZAP-70 recruitment by ezrin and CD43 removal by moesin. *J Cell Biol* **179:** 733–746

Ilani T, Vasiliver-Shamis G, Vardhana S, Bretscher A, Dustin ML (2009) T cell antigen receptor signaling and immunological synapse stability require myosin IIA. *Nat Immunol* **10:** 531–539

Infantino S, Benz B, Waldmann T, Jung M, Schneider R, Reth M (2010) Arginine methylation of the B cell antigen receptor promotes differentiation. *J Exp Med* **107:** 5094–5099

Kuhn JR, Poenie M (2002) Dynamic polarization of the microtubule cytoskeleton during CTL-mediated killing. *Immunity* **16:** 111–121

Kunda P, Pelling AE, Liu T, Baum B (2008) Moesin controls cortical rigidity, cell rounding, and spindle morphogenesis during mitosis. *Curr Biol* **18:** 91–101

Ludford-Menting MJ, Oliaro J, Sacirbegovic F, Cheah ET, Pedersen N, Thomas SJ, Pasam A, Iazzolino R, Dow LE, Waterhouse NJ, Murphy A, Ellis S, Smyth MJ, Kershaw MH, Darcy PK, Humbert PO, Russell SM (2005) A network of PDZ-containing proteins regulates T cell polarity and morphology during migration and immunological synapse formation. *Immunity* **22:** 737–748

Lue RA, Brandin E, Chan EP, Branton D (1996) Two independent domains of hDlg are sufficient for subcellular targeting: the PDZ1-2 conformational unit and an alternatively spliced domain. *J Cell Biol* **135:** 1125–1137

Mossman KD, Campi G, Groves JT, Dustin ML (2005) Altered TCR signaling from geometrically repatterned immunological synapses. *Science* **310:** 1191–1193

Naba A, Reverdy C, Louvard D, Arpin M (2008) Spatial recruitment and activation of the Fes kinase by ezrin promotes HGF-induced cell scattering. *EMBO J* **27:** 38–50

Ng T, Parsons M, Hughes WE, Monypenny J, Zich D, Gautreau A, Arpin M, Gschmeissner S, Verveer PJ, Bastiens PIH, Parker PJ (2001) Ezrin is a downstream effector of trafficking PKC-integrin

complexes involved in the control of cell motility. *EMBO J* **20**: 2723–2741

Nguyen K, Sylvain NR, Bunnell SC (2008) T cell costimulation via the integrin VLA-4 inhibits the actin-dependent centralization of signaling microclusters containing the adaptor SLP-76. *Immunity* **28**: 810–821

Olivo-Marin JC (2002) Extraction of spots in biological images using multiscale products. *Pattern Recognit* **35**: 1989–1996

Perez OD, Kinoshita S, Hitoshi Y, Payan DG, Kitamura T, Nolan GP, Lorens JB (2002) Activation of the PKB/AKT pathway by ICAM-2. *Immunity* **16**: 51–65

Poullet P, Gautreau A, Kadaré G, Girault JA, Louvard D, Arpin M (2001) Ezrin interacts with focal adhesion kinase and induces its activation independently of cell-matrix adhesion. *J Biol Chem* **276**: 37686–37691

Pujuguet P, Del Maestro L, Gautreau A, Louvard D, Arpin M (2003) Ezrin regulates E-cadherin-dependent adherens junction assembly through Rac1 activation. *Molec Biol Cell* **14**: 2181–2191

Roumier A, Olivo-Marin JC, Arpin M, Michel F, Martin M, Mangeat P, Acuto O, Dautry-Varsat A, Alcover A (2001) The membrane-microfilament linker ezrin is involved in the formation of the immunological synapse and in T cell activation. *Immunity* **15**: 715–728

Round JL, Humphries LA, Tomassian T, Mittelstadt P, Zhang M, Miceli MC (2007) Scaffold protein Dlgh1 coordinates alternative p38 kinase activation, directing T cell receptor signals toward NFAT but not NF-kappaB transcription factors. *Nat Immunol* **8**: 154–161

Round JL, Tomassian T, Zhang M, Patel V, Schoenberger SP, Miceli MC (2005) Dlgh1 coordinates actin polymerization, synaptic T cell receptor and lipid raft aggregation, and effector function in T cells. *J Exp Med* **201**: 419–430

Ruppelt A, Mosenden R, Gronholm M, Aandahl EM, Tobin D, Carlson CR, Abrahamsen H, Herberg FW, Carpen O, Tasken K (2007) Inhibition of T cell activation by cyclic adenosine 5′-monophosphate requires lipid raft targeting of protein kinase a type I by the a-kinase anchoring protein Ezrin. *J Immunol* **179**: 5159–5168

Savage NDG, Kimzey SL, Bromley SK, Johnson KG, Dustin ML, Green JM (2002) Polar redistribution of the sialoglycoprotein CD43: implications for T cell function. *J Immunol* **168**: 3740–3746

Shaffer MH, Dupree RS, Zhu P, Saotome I, Schmidt RF, McClatchey AI, Freedman BD, Burkhardt JK (2009) Ezrin and moesin function together to promote T cell activation. *J Immunol* **182**: 1021–1032

Soderberg O, Gullberg M, Jarvius M, Ridderstrale K, Leuchowius KJ, Jarvius J, Wester K, Hydbring P, Bahram F, Larsson LG, Landegren U (2006) Direct observation of individual endogenous protein complexes *in situ* by proximity ligation. *Nat Methods* **3**: 995–1000

Sperling AI, Sedy JR, Manjunath N, Kupfer A, Ardam B, Burkhardt JK (1998) TCR signaling induces selective exclusion of CD43 from the T cell-antigen presenting cell contact site. *J Immunol* **161**: 6459–6462

Takahashi K, Sasaki T, Mammoto A, Takaishi K, Kameyama T, Tsukita S, Tsukita S, Takai Y (1997) Direct interaction of the Rho dissociation inhibitor with ezrin/radixin/moesin initiates the activation of the Rho small G protein. *J Biol Chem* **272**: 23371–23375

Thoulouze MI, Sol-Foulon N, Blanchet F, Dautry-Varsat A, Schwartz O, Alcover A (2006) Human immunodeficiency virus type-1 infection impairs the formation of the immunological synapse. *Immunity* **24**: 547–561

Treanor B, Depoil D, Gonzalez-Granja A, Barral P, Weber M, Dushek O, Bruckbauer A, Batista FD (2010) The membrane skeleton controls diffusion dynamics and signaling through the B cell receptor. *Immunity* **32**: 187–199

Urzainki A, Serrador JM, Viedma F, Yanez-Mo M, Rodriguez A, Corbi AL, Alonso-Lebrero JL, Luque A, Deckert M, Vazquez J, Sanchez-Madrid F (2002) ITAM-based interaction of ERM proteins with Syk mediates signaling by the leukocyte adhesion receptor PSLG-1. *Immunity* **17**: 401–412

Varma R, Campi G, Yokosuka T, Saito T, Dustin ML (2006) T cell receptor-proximal signals are sustained in peripheral microclusters and terminated in the central supramolecular activation cluster. *Immunity* **25**: 117–127

Xavier R, Rabizadeh S, Ishiguro K, Andre N, Ortiz JB, Wachtel H, Morris DG, Lopez-Ilasaca M, Shaw AC, Swat W, Seed B (2004) Discs large (Dlg1) complexes in lymphocyte activation. *J Cell Biol* **166**: 173–178

Yablonski D, Kuhne MR, Kadlecek T, Weiss A (1998) Uncoupling of nonreceptor tyrosine kinases from PLC-gamma1 in an SLP-76-deficient T cell. *Science* **281**: 413–416

Yokosuka T, Kobayashi W, Sakata-Sogawa K, Takamatsu M, Hashimoto-Tane A, Dustin ML, Tokunaga M, Saito T (2008) Spatiotemporal regulation of T cell costimulation by TCR-CD28 microclusters and protein kinase C theta translocation. *Immunity* **29**: 589–601

Yokosuka T, Sakata-Sogawa K, Kobayashi W, Hiroshima M, Hashimoto-Tane A, Tokunaga M, Dustin ML, Saito T (2005) Newly generated T cell receptor microclusters initiate and sustain T cell activation by recruitment of Zap70 and SLP-76. *Nat Immunol* **6**: 1253–1262